Electronic Supplemental Information

Extended quinoid molecule based on bis(thiophene-diketopyrrolopyrrole) with balanced ambipolar semiconducting property and strong near-infrared absorption

Wansong Shang,[a, b] Guangchao Han,[a, b] Qingrui Fan, [c] Xiaobo Yu, [a, b] Dongsheng Liu, [a, b] Cheng Li,[a, b] Xi-Sha Zhang,[a, b] Yuanping Yi,[a, b] Guanxin Zhang,* [a, b] Deqing Zhang* [a, b]

Table of Contents

1. Materials and characterization techniques

Commercial reagents were used as received, unless otherwise indicated. Compound DPP-Br was purchased from SunaTech Inc., Jiangsu, China.

^{1}HNMR and ^{13}CNMR spectra were measured on Bruker AVANCE III 400 MHz and 700 MHz spectrometers. Tetramethylsilane (TMS) served as the internal standard for ^{1}H NMR, and $CDCl_3$ or CD_2Cl_2 served as the internal standard for ^{13}C NMR. The following abbreviations were used to express the multiplicities: s = singlet; d= doublet; m = multiplet; br = broad. Matrix assisted laser desorption/ionization time-of-flight (MALDI-FTICR) mass spectra were collected on a Bruker Solarix-XR high-resolution mass spectrometer. Melting points were measured on a BÜCHI melting point B-540. Elemental analysis was conducted on a Carlo-Erba-1106 instrument. Ultraviolet-visible-NIR absorption spectra were carried out on a Shimadzu UV-2600 spectrophotometer. Cyclic voltammetric measurements were carried out in a three-electrode cell by using glassy carbon as the working electrode, a Pt as auxiliary electrode, and an Ag/AgCl (saturated KCl) as reference electrode on a computer-controlled CHI660C instrument at room temperature; the scan rate was 100 mV s^{-1}, and nBu_4NPF_6 was used as the supporting electrolyte. For calibration, the redox potential of ferrocene/ ferrocenium (Fc/Fc^{+}) was measured under the same conditions. Thermogravimetric analysis (TGA) measurements were carried out on a PerkinElmer series 7 thermal analysis system under N_2 at a heating rate of 10 ^{o}C min^{-1}. Atomic-force microscopy images were taken by using a Digital Instruments Nanoscope V atomic force microscope operated in tapping mode with a Nanoscope V instrument in air. XRD measurements were performed at the Panalytical empyrean, using X-rays with a wavelength of λ = 1.54 Å.

2. TGA analysis

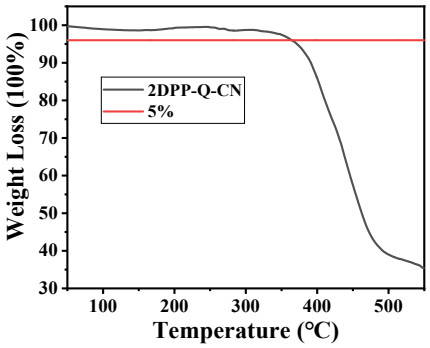

Figure S1 TGA curve for 2DPP-Q-CN, recorded at a heating and cooling rate (50-550 °C) of 10 °C min^{-1} under nitrogen.

3. Theoretical calculations

The ground-state geometry of 2DPP-Q-CN was optimized by density functional theory (DFT) at the B3LYP/6-31G(d, p) level. To simplify the calculation, the alkyl chains are replalced by methyl groups. Then, the vertical excitations were calculated by time-dependent DFT at the same level with the polarizable continuum model for chloroform.

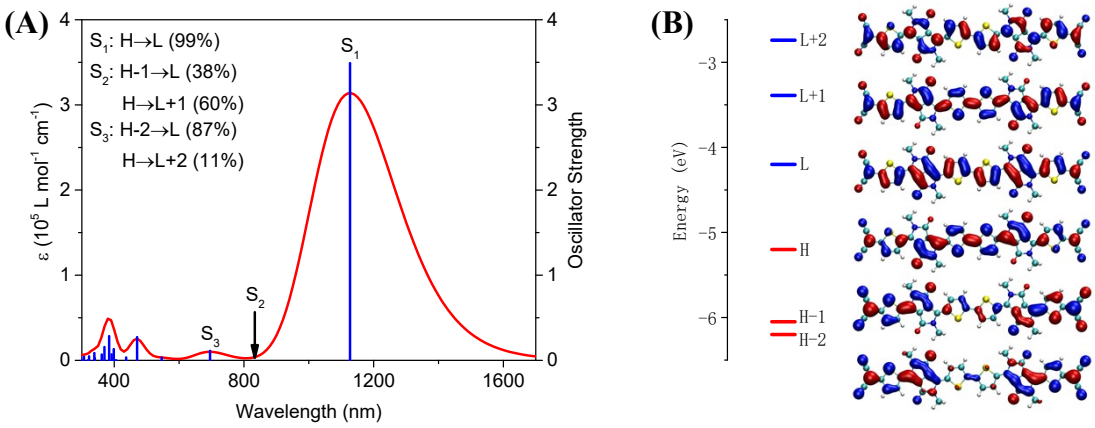

Figure S2 A) Simulated absorption spectrum of 2DPP-Q-CN; B) The frontier molecular orbitals of 2DPP-Q-CN and corresponding energy levels.

4. The cyclic voltammograms

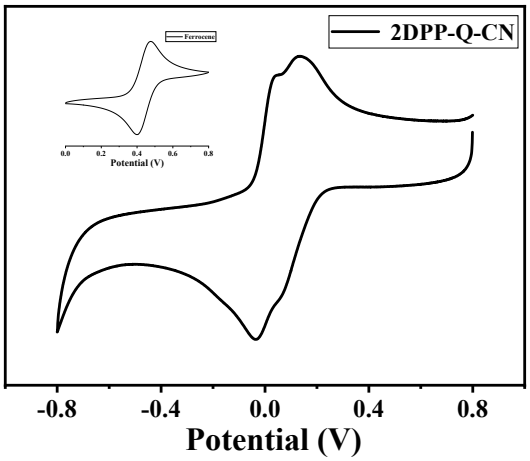

Figure S3 Cyclic voltammogram of 2DPP-Q-CN in CH_2Cl_2 solution (1 mM) with scan rate of 100 mV s^{-1}. The inset shows the cyclic voltammograms of ferrocene under the same condition.

5. Ultraviolet Photoelectron Spectroscopy (UPS) and Inverse Photoemission Spectroscopy (IPES) measurements.

The UPS measurement was conducted a Kratos ULTRA AXIS DLD photoelectron spectroscopy system with an ultra-high vacuum of 3×10^{-9} Torr. He-discharge lamp (21.22 eV) excitation sources were taken as excitation source. The IPES measurement was performed using a customized ULVAC-PHI LEIPS instrument with Bremsstrahlung isochromatic mode. The samples were fabricated by spin-coating method as follows: 2DPP-Q-CN was dissolve in chloroform (10 mg/mL) and spin-coating on ITO substrate at 2000 rpm for 60 s.

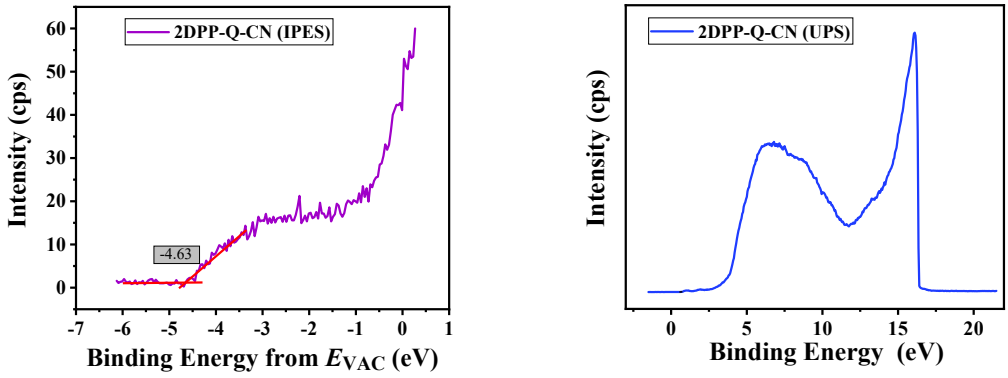

Figure S4 IPES (*left*) and UPS (*right*) spectra of 2DPP-Q-CN thin film

6. FET device fabrication and characterization

FETs with a top-gate/bottom-contact (TGBC) configuration were fabricated on heavily doped silicon wafers covered with 300 nm thick silicon dioxide layers. The drain–source (D–S) gold contacts were fabricated by photolithography. The substrates were first cleaned by acetone and water, then immersed in Piranha solution (2: 1 mixture of sulfuric acid and 30% hydrogen peroxide). The substrates were further rinsed with deionized water and isopropyl alcohol for several times and subsequently dried under vacuum at 80 ^{o}C, after that the silica substrates were modified with octadecyltrichlorosilane (OTS). They were washed with *n*-hexane, $CHCl_3$ and isopropyl alcohol sequentially. Compound 2DPP-Q-CN was dissolved in $CHCl_3$ (10 mg mL^{-1}), and spin-coating on the substrate at 2000 rpm for 60 s. The annealing process was carried out in a nitrogen box for 10 min at different temperatures. Polymethylmethacrylate (PMMA, Mw = 996 kDa) solution in anhydrous n-butyl acetate (60 mg/mL) was spin-coated on the surface of the polymer layer to give PMMA thin films (PMMA thickness~900 nm, Ci = 2.56 nF/cm^2) , followed by thermal annealing at 90 ^{o}C for 60 min in a nitrogen box. The aluminum gate electrode (~ 80 nm) was deposited on the dielectric layer by a vacuum deposition method.

All measuring processes were performed under ambient conditions with a relative humidity of 20~40%. The FET device performance was evaluated on a Keithley 4200 SCS semiconductor parameter analyzer on a probe stage. The carrier mobility (μ) was calculated from the data in the saturated regime according to the equation:

$$I_{DS} = (W/2L)\,\mu_{sat} C_i\,(V_G - V_T)^2$$

where I_{DS} is the saturation drain current, W/L is the channel width/length, C_i is the capacitance per unit area of the gate dielectric layer, and V_G and V_T are the gate voltage and the threshold voltage, respectively. The channel length and channel width of the FET devices were 5 μm and 1440 μm, respectively.

Table S1 Hole mobilities (μ_h), electron mobilities (μ_e), threshold voltages (V_T), and current on/off ratios (I_{on}/I_{off}) for OFET devices based on thin-films of 2DPP-Q-CN after annealing at different temperatures.

Annealing temp.(°C)	μ_h[a] [$cm^2V^{-1}s^{-1}$]	V_T [V]	I_{on}/I_{off}	μ_e[a] [$cm^2V^{-1}s^{-1}$]	V_T [V]	I_{on}/I_{off}
100°C	3.5×10^{-5} / 1.6×10^{-6}	-40 ~ -60	10	1.2×10^{-5} / 5.1×10^{-6}	30 ~ 40	10
120°C	0.19 / 0.16	-50 ~ -70	10	0.20 / 0.17	30 ~ 50	10

[a] The hole/electron mobilities were provided in 'highest/average' form, and the highest and average data are based on 10 different OFET devices.

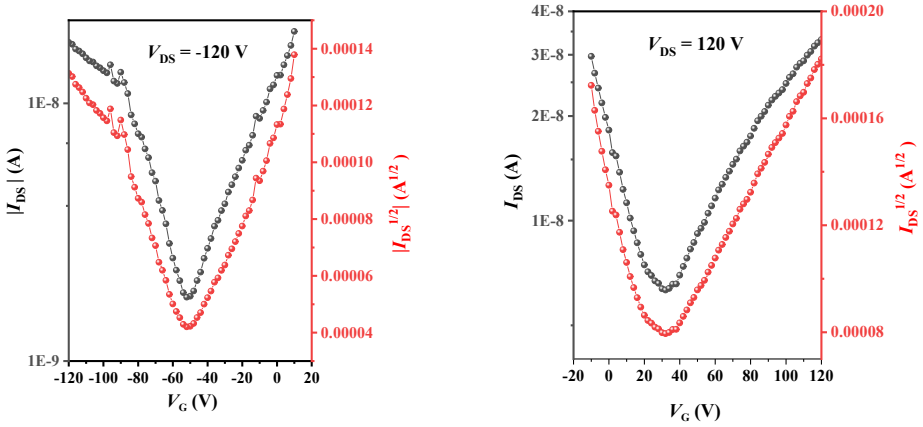

Figure S5 Transfer curves of thin film OFET device of 2DPP-Q-CN after annealing at 100 °C for 10 min.

7. X-ray diffraction (XRD) and atomic force microscopy (AFM)

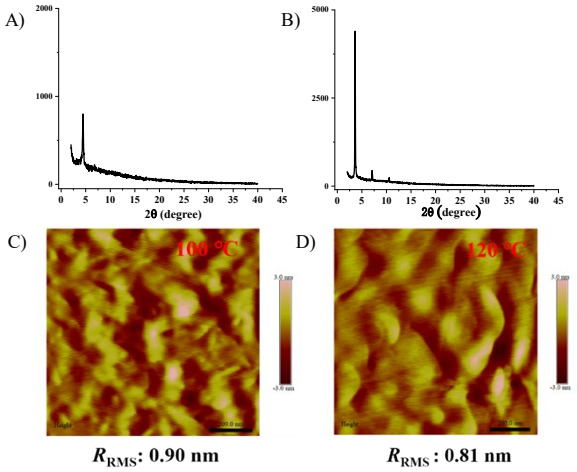

Figure S6 XRD pattern (A, B) and AFM images (C, D) of the 2DPP-Q-CN thin film after annealing at 100 °C (A, C) or 120 °C (B, D) for 10 min.

8. NMR spectra

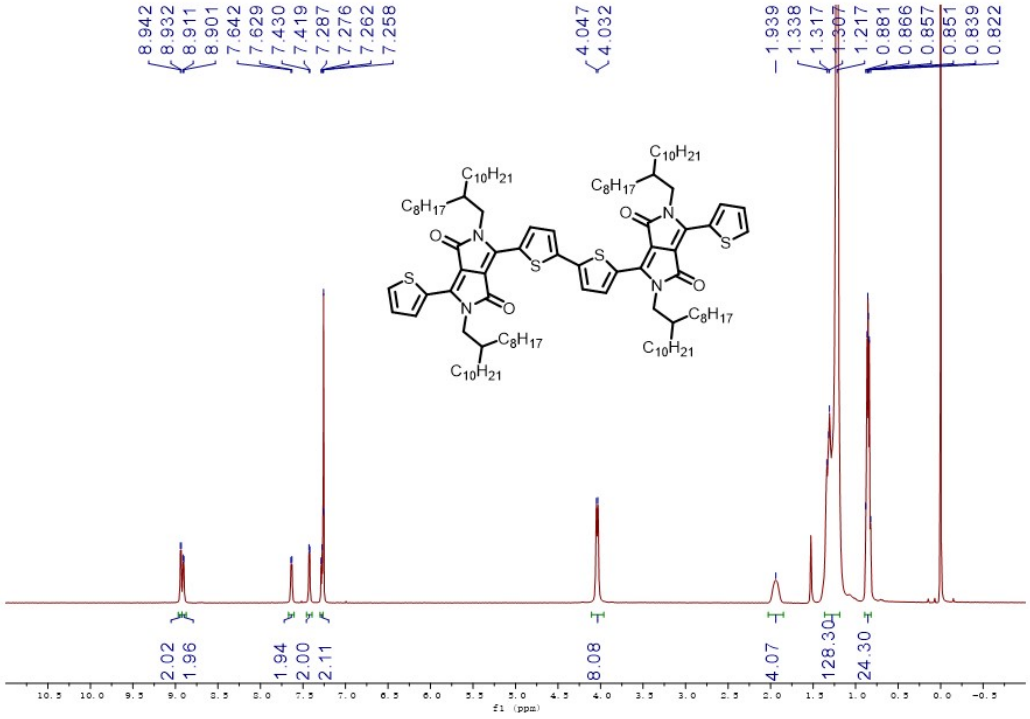

Figure S7 ^{1}H NMR spectrum of 2DPP in $CDCl_3$

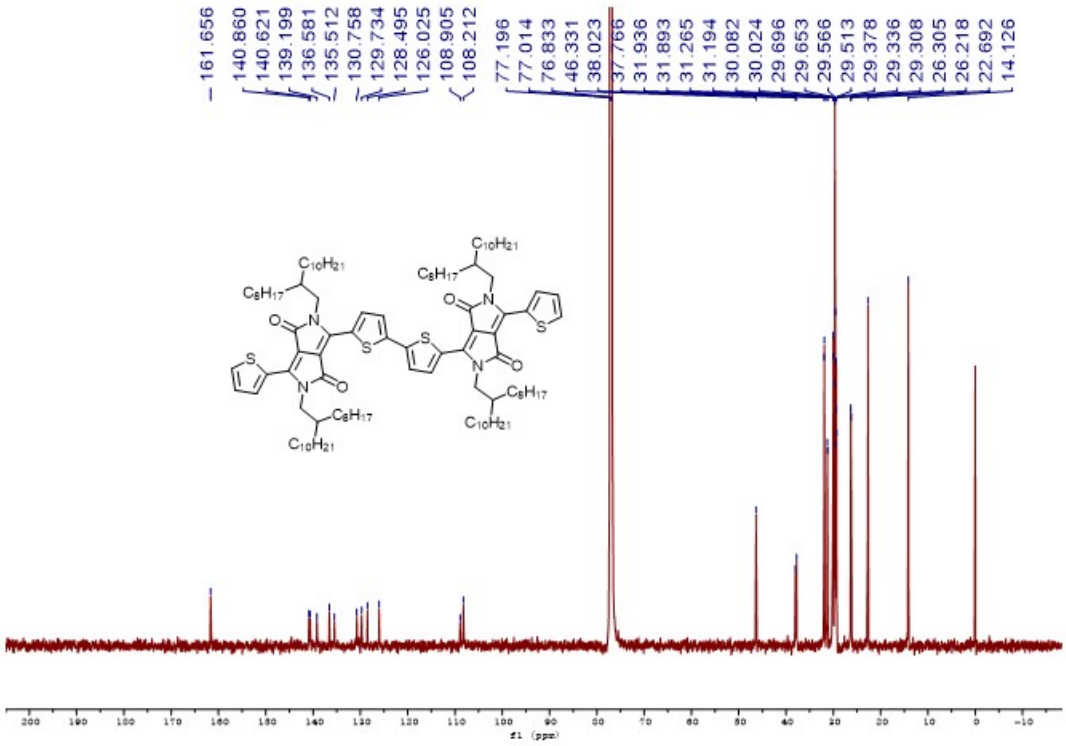

Figure S8 ^{13}C NMR spectrum of 2DPP in $CDCl_3$

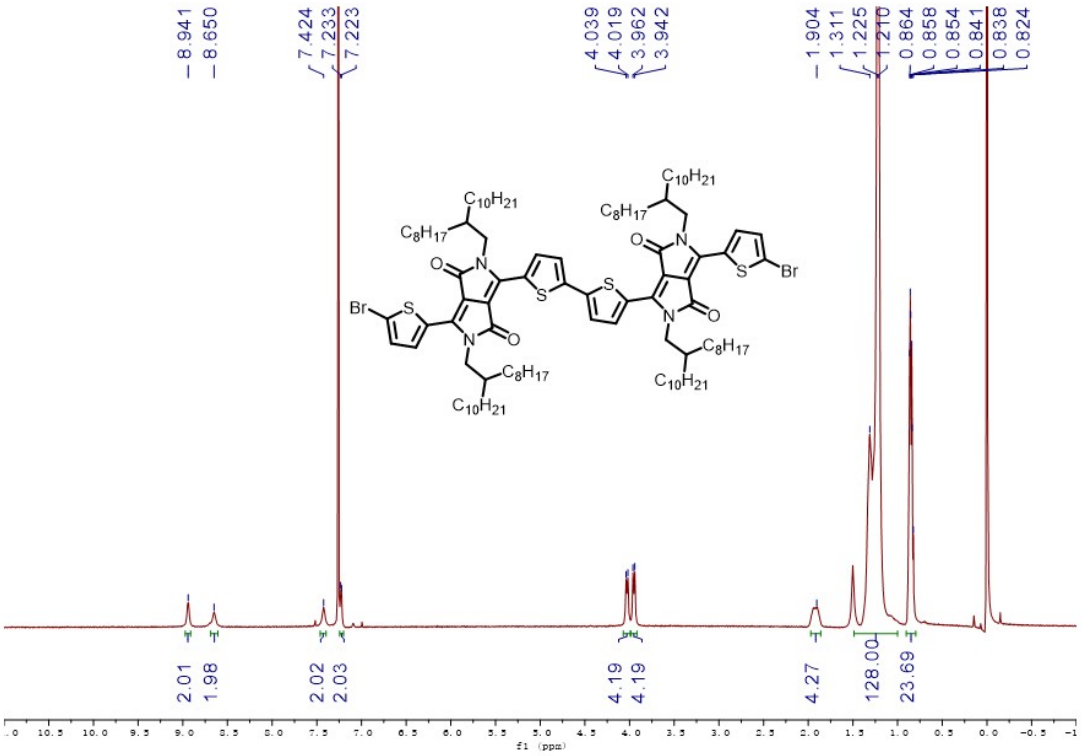

Figure S9 ^{1}H NMR spectrum of 2DPP-2Br in $CDCl_3$

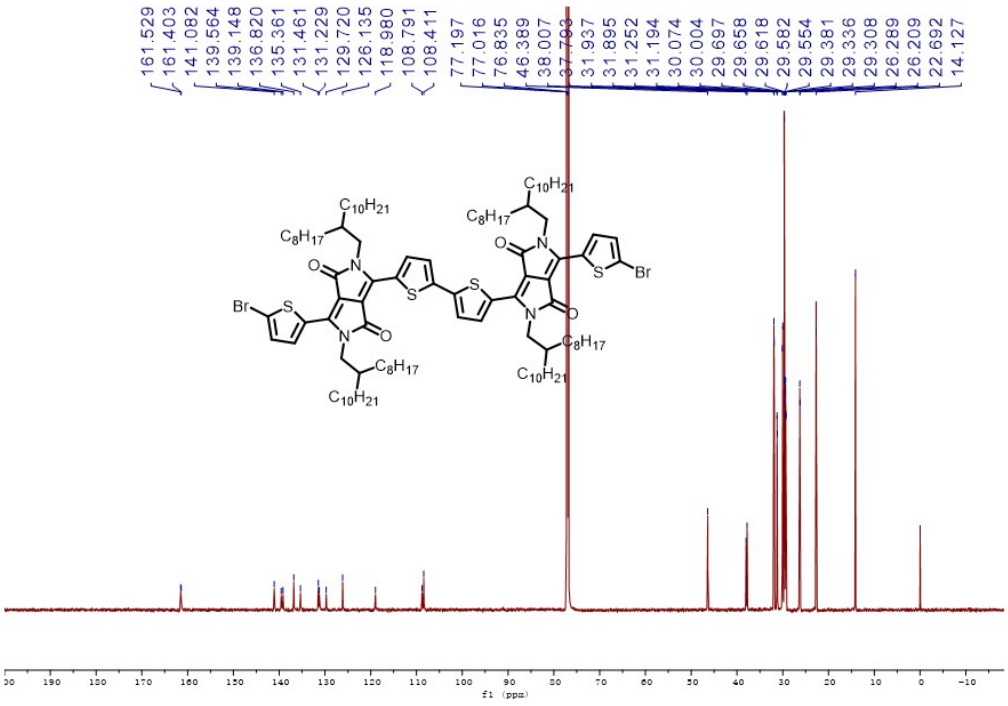

Figure S10 ^{13}C NMR spectrum of 2DPP-2Br in $CDCl_3$

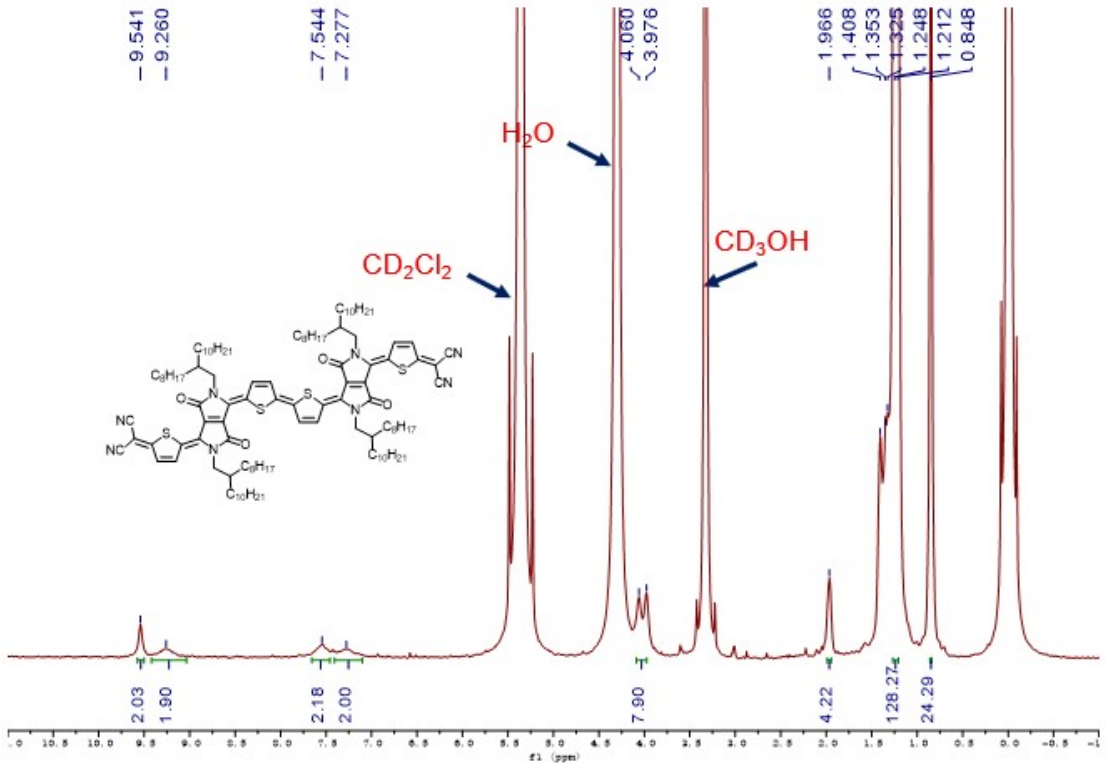

Figure S11 ^{1}H NMR spectrum of 2DPP-Q-CN at 253.2 K in CD_2Cl_2 with a drop of CD_3OH

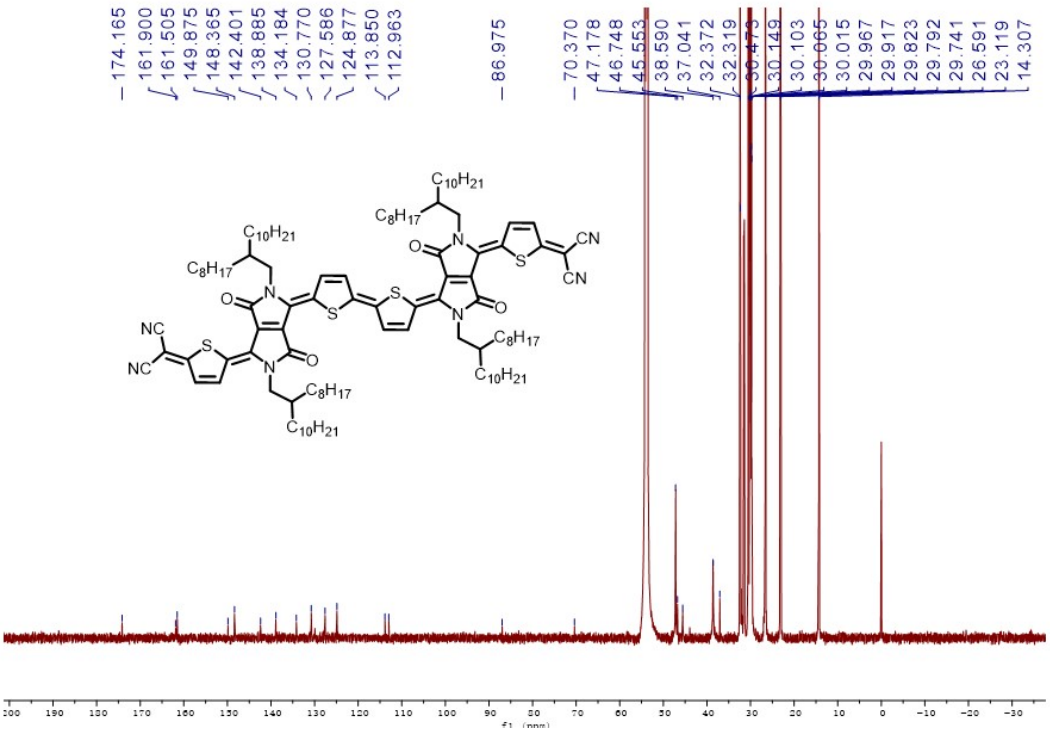

Figure S12 ^{13}C NMR spectrum of 2DPP-Q-CN in CD_2Cl_2

9. HRMS spectrum

MALDI,9-9-1,20221018

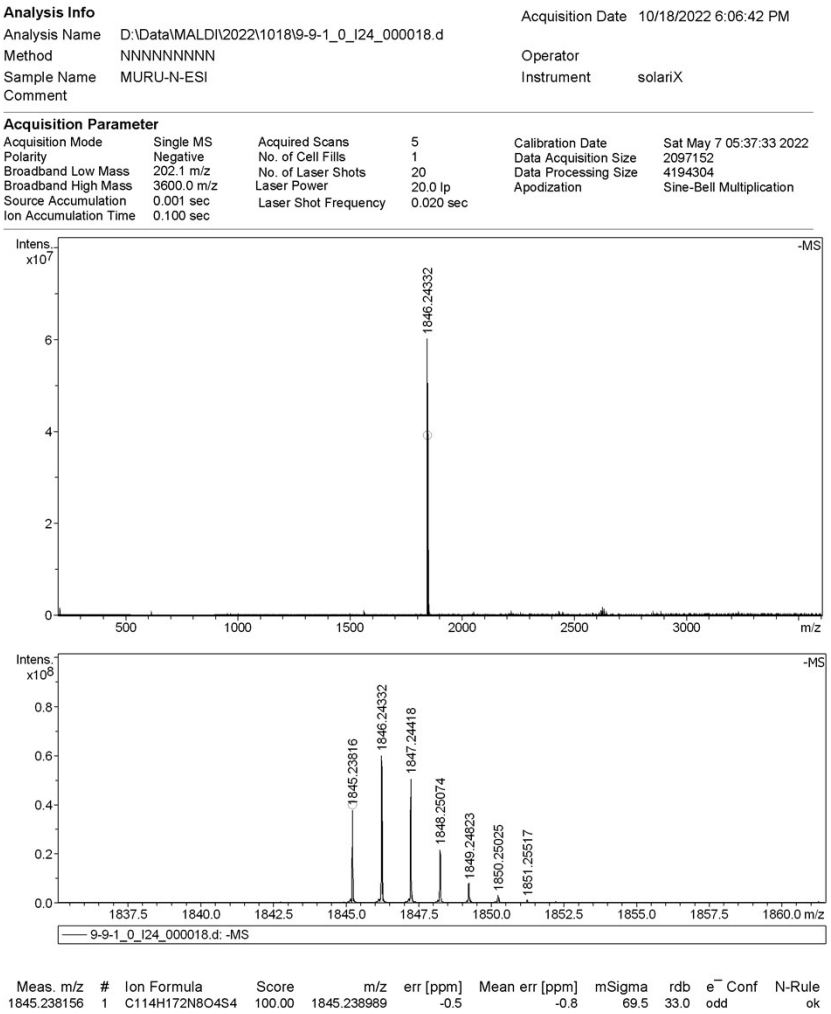

Figure S13 HRMS spectrum of 2DPP-Q-CN

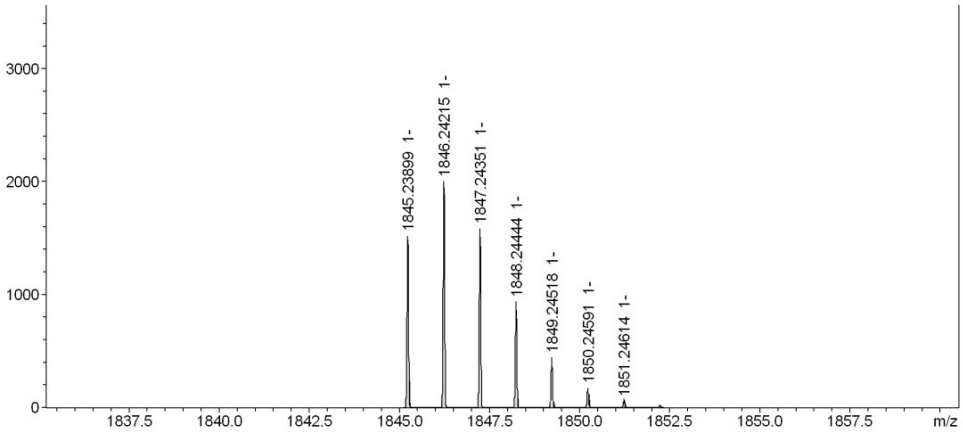

Figure S14 Calculated isotopic distribution pattern for 2DPP-Q-CN.